Inside baleen: Exceptional microstructure preservation in a late Miocene whale skeleton from Peru
Gioncada et al.

Figure DR1. Cerro Colorado geological map and stratigraphic section modified from Bianucci et al. (2016), showing the distribution of fossil mysticetes and the position of M1. The position of *Lyviatan melvillei* holotype finding is also reported.

Reference cited

Bianucci, G., Celma C., Landini W., Post K., Tinelli C., de Muizon C., Gariboldi K., Malinverno E., Cantalamessa G., Gioncada A., Collareta A., Gismondi R., Varas-Malca R., Urbina M. and Lambert O., 2016, Mapping and vertical distribution of fossil marine vertebrates in Cerro Colorado, the type locality of the giant raptorial sperm whale *Livyatan melvillei* (Miocene, Pisco Formation, Peru): Journal of Maps, v. 12, p. 543–557, doi:10.1080/17445647.2015.1048315.

Additional paleontological observations on the balaenopteroid whale skeleton M1

M1 displays a high degree of articulation, e.g.: both mandibles are still in anatomic connection with the cranium; the forelimbs show perfectly articulated carpal and metacarpal bones; the exposed segment of vertebral column presents articulated vertebrae; the bony thorax (thoracic vertebrae and ribs) preserves its three-dimensional architecture (see figure below).

The skull, mandibles, and ear bones of M1, which are divided into several blocks and fragments, display a typically balaenopteroid outline. A bizygomatic width of ca 96 cm has been estimated for M1. This measurement allows calculating a total body length of ca 8.5 m based on the equation proposed by Lambert et al. (2010). Based on the presence of vertebral epiphyses ankylosed to the relative apophyses, M1 is regarded as a fully grown adult individual; as such, it is here attributed to the undescribed middle-sized (ca 7-9 m long) balaenopteroid species recognized at Cerro Colorado by Collareta et al. (2015).

Figure DR2. The bony thorax (thoracic vertebrae and ribs) of M1 preserves its three-dimensional architecture attesting the high degree of articulation of the fossil mysticete skeleton (long dimension of the photo is about 1 m).

References cited

Collareta, A., Landini W., Lambert O., Post K., Tinelli C., Di Celma C., Panetta D., Tripodi M., Salvadori P.A., Caramella D., Marchi D., Urbina M., Bianucci G., 2015, Piscivory in a Miocene Cetotheriidae of Peru: first record of fossilized stomach content for an extinct baleen-bearing whale: The Science of Nature, v. 102, article no. 70, doi:10.1007/s00114-015-1319-y.

Lambert, O., Bianucci, G., Post, K., de Muizon, C., Salas-Gismondi, R., Urbina, M., and Reumer, J., 2010, The giant bite of a new raptorial sperm whale from the Miocene epoch of Peru: Nature, v. 466, p. 105–108, doi:10.1038/nature09067.

Material preparation, analytical methods and data

Material preparation and analytical methods

Small pieces of the concretion holding plate-like structures were mounted in resin and sectioned, orthogonally to and along the grooves; one fragment holding bristles was gently crushed to expose the delicate strings. Some phosphatic material was collected from the fossil bristles with a needle and powdered for X-rays diffraction analysis (XRPD). Some fragments were mounted in resin within tube-like holders and polished exposing a section of the string orthogonal to its long axis; others were mounted without resin. The mounts were carbon-coated for scanning electron microscopy with backscattered electrons imaging and energy-dispersive X-ray spectroscopy (SEM-EDS, Philips XL30 SEM equipped with DX4i EDAX microanalysis) and wavelength-dispersive spectroscopy electron probe microanalysis (WDS-EPMA, Cameca SX50 instrument at CNR, Rome, Italy). X-ray powder diffraction (XRPD) data were collected on a Bruker D2 Phaser diffractometer operating at 10 mA and 30 kV, using a flat background-free sample holder and Cu Kα radiation with $\lambda = 1.54178$ Å. Data were processed using the software DIFFRAC.EVA V4.1.

Data

SEM-EDS

Through SEM-EDS analysis, the concretion forming the plates casts and containing fossil bristles was carefully investigated to identify the fossil evidence of tubules and their mineral composition. Analytical conditions were 20 kV accelerating voltage, 5 nA beam current.
The well cemented diatomaceous sediment encasing free bristles (Fig. 2b in the paper) has >95% of diatom frustules and minor terrigenous particles; 95% of the diatom assemblage is made of *Stephanopyxis* spp. and frustule outlines lack any indication of diagenetic compression. In the enlargement here below (A), *Azpeitia* sp. frustule can be recognized; silica is preserved and details of the frustules ultrastructure are still visible; white arrow indicates diamond-shaped areolae on the

mantle and no signs of diagenetic compression are found (SEM-SE). In B, an example of Ca-phosphate and dolomite identification by SEM in a sectioned fossil bristle is shown. The brighter area corresponds to Ca-phosphate permeated by late gypsum (SEM-BSE).

Figure DR3_1
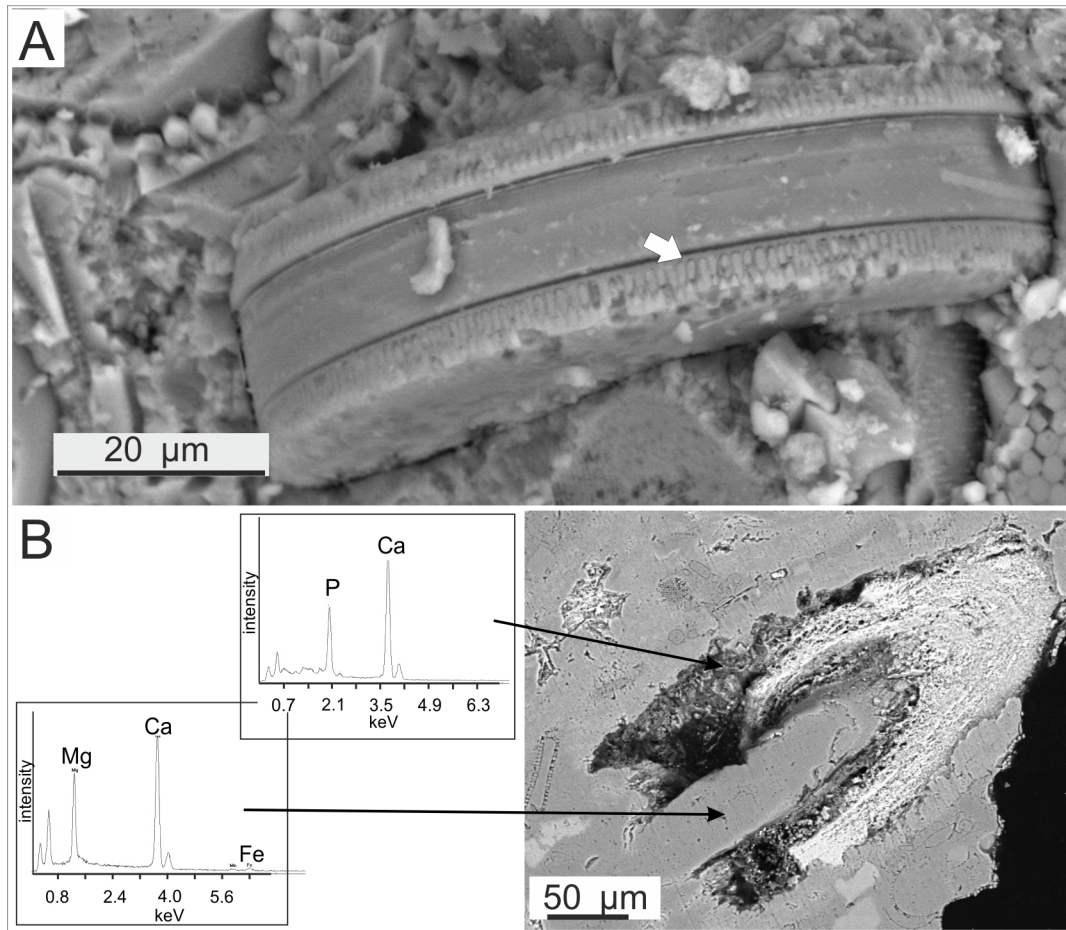
X-rays DIFFRACTION

The sample was manually selected under binoculars. A preliminary X-ray diffraction powder (XRPD) pattern indicated that the occurring main phases were dolomite, gypsum and quartz. The same sample was gently ground in water; after two hours the water was removed and the sample was dried at 80°C in a furnace. The final XRPD pattern is reported in Figure DR3_2(a); the identified phases were dolomite, quartz, minor amounts of orthopyroxenes, amphibole and plagioclase, and, as emphasized in Figure DR3_2(b), apatite-(CaF) ('fluorapatite'). In the enlarged portion of

the XRPD pattern, only the 'fluorapatite' peaks not superimposed to indexed peaks of other phases are reported.

Figure DR3_2
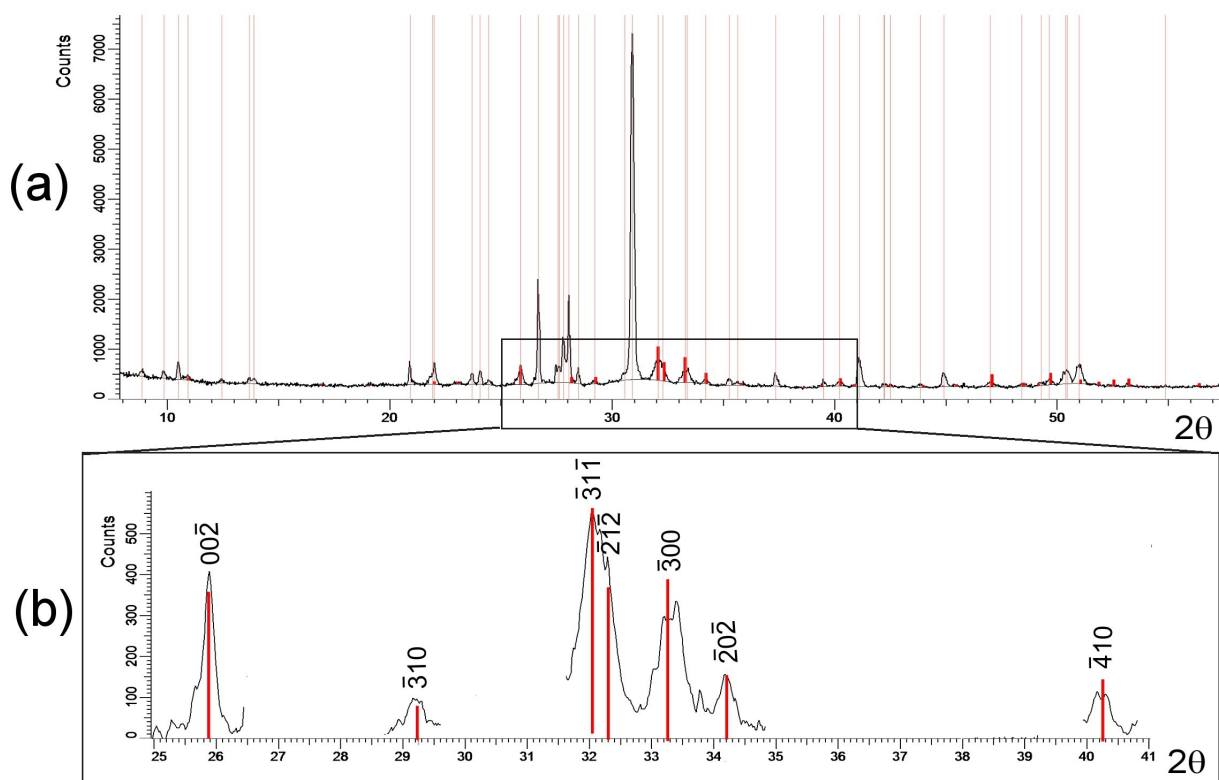
ELECTRON MICROPROBE

EPM analyses of Ca-phosphate of the bristles and of the dolomite are reported in Table DR3_1 (below). The Ca-phosphate analyses give values for the Ca/P atomic ratio which are higher compared to hydroxyapatite composition (Wopenka and Pasteris, 2005), but in the range of published bioapatite bone materials (Li and Pasteris, 2014). The occurrence of low amounts of sulfur in analyses 1-4, joined to the relatively high Ca content, could be due to the pervasive occurrence of gypsum within porosity. We attribute the low totals of Ca-phosphate compared to published EMPA data (Li and Pasteris, 2014) to the imperfect surface obtained when polishing such porous material.

	Ca-phosphate				dolomite			
	1	2	3	4	5	6	7	8
wt%								
SO_3	1.84	1.99	1.48	1.64	0.02	bdl	0.03	0.06
P_2O_5	31.28	31.42	30.38	31.94	0.06	0.09	0.12	0.18
SiO_2	1.34	1.49	1.43	1.77	0.02	bdl	0.06	0.01
Fe_2O_3tot	0.06	0.12	0.05	0.10	0.06	0.02	0.02	0.05
MgO	1.06	1.21	1.15	1.26	21.69	20.79	20.48	21.06
CaO	44.35	44.93	44.35	45.13	31.98	31.29	31.55	31.42
MnO	0.04	0.05	0.05	0.05	0.03	0.03	bdl	0.05
SrO	0.14	0.30	0.16	0.15	0.13	0.15	0.01	0.14
PbO	bdl	bdl	0.03	bdl	0.06	bdl	bdl	0.00
Na_2O	0.90	1.01	0.95	0.91	0.07	0.09	0.04	0.08
F	2.86	2.86	3.14	2.88	0.08	bdl	0.08	0.01
Cl	0.13	0.11	0.20	0.20	0.01	0.02	0.01	0.02
sum	84.01	85.48	83.34	86.02	54.20	52.47	52.40	53.06
Ca/P atomic ratio	1.80	1.81	1.85	1.79				

Table DR1. Electron probe WDS analyses of the phosphatic material now forming the bristles (1-4) and of the dolomite cementing the concretion (5-8); bdl: below detection limit; Fe_2O_3tot: all Fe as Fe_2O_3. Analytical conditions: 15kV accelerating voltage, 5 nA beam current. A 10 micron defocused beam was used.

References cited

Li, Z., Pasteris, J.D., 2014, Tracing the pathway of compositional changes in bone mineral with age: Preliminary study of bioapatite aging in hypermineralized dolphin's bulla: Biochimica et Biophysica Acta, v. 1840, p. 2331–2339.

Wopenka, B., Pasteris, J.D., 2005, A mineralogical perspective on the apatite in bone: Materials Science and Engineering, C 25, p.131–143.